JOURNAL OF GEOPHYSICAL RESEARCH, VOL. 106, NO. D11, PAGES 11,835–11,848, JUNE 16, 2001

Stratospheric filamentation into the upper tropical troposphere

R. K. Scott, J.-P. Cammas, P. Mascart, and C. Stolle

Laboratoire d'Aérologie, Toulouse, France

Abstract. We investigate the process of Rossby wave breaking on the subtropical tropopause and the resulting filamentary structures of stratospheric air transported into the upper tropical troposphere. We make extensive use of the Measurements of Ozone by Airbus In-Service Aircraft (MOZAIC) flight database, both for identifying individual wave-breaking events and for analyzing the small-scale features of the filamentation process. Two models are used to provide a dynamically consistent description of the evolution of a particular wave-breaking event, one a limited area, high-resolution general circulation model, MesoNH, the other an isentropic contour advection model. The ability of both of these to represent the small-scale evolution of the filament is examined by explicit comparison with the MOZAIC ozone data; at larger scales, comparison is made with analyses from the European Centre for Medium-Range Weather Forecasts. Two other wave-breaking events are presented briefly, on the one hand, verifying that the filamentary structure is ubiquitous, on the other hand, illustrating additional, distinct features of the evolution. A simple analysis of all the MOZAIC flights over the southern tropical Atlantic provides an indication of the frequency of wave-breaking events over this region. Together with the small-scale development suggested by the model studies and present in the MOZAIC data we infer a potentially significant contribution to the global stratosphere-troposphere exhange from the wave-breaking processes.

1. Introduction

The chemical compositions of the stratosphere and the troposphere play a crucial role in both stratospheric ozone destruction and in the radiative properties of the atmosphere. Since the chemical compositions in each are also very different, evaluating the stratosphere-troposphere exchange (STE) of air between one region and the other is crucial to our understanding of both the short- and the long-term behavior of the atmosphere. One important mechanism by which STE can occur is through the quasi-horizontal motion on those isentropic surfaces that intersect the tropopause. Since this motion is inhibited by the dynamical barrier at the tropopause [e.g., *Haynes and Shuckburgh*, 2000], which may be identified with the strong isentropic gradients of potential vorticity (PV) and chemical species, it is important to assess the strength of this barrier and the mechanisms by which it may be crossed (see *Holton et al.* [1995] for a recent review).

At high latitudes in the stratosphere the dynamical barrier associated with the strong isentropic PV gradients of the winter polar vortex has received considerable attention, including studies of vortex erosion and filamentation using a wide range of observations, theory, and numerical modeling [e.g., *Norton*, 1994; *Waugh et al.*, 1994; *McIntyre*, 1995]. Although it is widely accepted that in low latitudes and near the tropopause there is a similar dynamical barrier acting to inhibit mixing [e.g., *Polvani et al.*, 1995], the strength of this barrier is not well understood. Observational and modeling evidence suggests, however, that the barrier at low latitudes is weaker than that of the stratospheric polar vortex, consistent with the more dynamically active troposphere, and that substantial STE can occur in both directions [e.g., *Chen*, 1995; *Appenzeller et al.*, 1996].

In midlatitudes, where the tropopause intersects isentropes approximately in the 300–330 K range, STE can occur in regions of large tropopause deformation, or tropopause folds. These are associated with strong baroclinicity and upper level frontogenesis and typically result in deep intrusions of stratospheric air into the middle and even the lower troposphere. Numerous studies have been conducted recently examining the structure of, and the STE associated with, such events, including intensive observational campaigns [e.g., *Appenzeller and Davis.*, 1992; *Appenzeller et al.*, 1996] and numerical modeling [e.g., *Ebel et al.*, 1991; *Mariotti et al.*, 1997; *Bithell et al.*, 1999]. In the subtropics, where the tropopause intersects isentropes approximately in the 340–370 K range, STE can again result from tropopause folding events [e.g., *Gouget et al.*, 1996; *Baray et al.*, 2000]. In this region, however, strong tropopause deformation can also result from large-amplitude barotropic Rossby waves. The breaking of these waves can lead to STE through the irreversible deformation of the isentropic PV contours near tropopause and the pinching off of filaments of stratospheric air into the upper tropical troposphere [*Postel and Hitchman*,

Paper number 2001JD900049.
0148-0227/01/2001JD900049$09.00

1999; *Waugh and Polvani*, 2000]. Note that here, in contrast to tropopause folding events, strong baroclinicity is not an essential ingredient and the wave breaking can occur over a large (e.g., 340–370 K) vertical extent.

In this paper we consider a particular wave-breaking event and provide a detailed description of the resulting filamentary intrusions of stratospheric air into the upper tropical troposphere. Our work complements that of *Appenzeller et al.* [1996] and other studies referenced above, which have focused on the structure and development of low-latitude and midlatitude tropopause folds. We focus on the geographical region over the southern tropical Altantic, which is one of the regions identified by *Postel and Hitchman* [1999] and *Waugh and Polvani* [2000] as having a relatively high occurrence of such wave-breaking events (the other being over the Pacific). We further restrict attention to the summer hemisphere, identified by *Postel and Hitchman* [1999] as the preferred season for Rossby wave breaking in the subtropics (and see also section 5.3 below). This is also consistent with the study of *Chen* [1995], who found evidence of STE on the 350 K isentropic surface only in the summer hemisphere, in association with the summer monsoon circulation. We note that stratospheric intrusions in this and other subtropical regions could also be of interest to recent discussions conserning observed tropospheric ozone and its seasonal and geographical variability [e.g., *Diab et al.*, 1996, and references therein].

We make use of ozone and other data gathered by several Measurements of Ozone by Airbus In-Service Aircraft (MOZAIC) [*Marenco et al.*, 1998] flights between Europe and South America that cross the tropical Atlantic in the upper troposphere. These provide high-resolution, along-trajectory measurements of quantities such as ozone mixing ratio, potential temperature, relative humidity, wind speed, and wind direction. European Centre for Medium-Range Weather Forecasts (ECMWF) analyzed fields and Meteosat imagery of water vapor are used to consider the synoptic situations in which the MOZAIC measurements are made.

We also use two kinds of numerical models to obtain a detailed description of the evolution of one such wave-breaking event, in which stratospheric air is advected deep into the tropics. One model is a high-resolution limited area nonhydrostatic (anelastic) model, MesoNH, [*Lafore et al.*, 1998; *Mallet et al.*, 1999] with a full suite of physical parameterizations; the other is an isentropic Lagrangian advection model, the contour advection with surgery (CAS) model [*Dritschel*, 1989]. A secondary aim of the paper is to examine the utility of these models for studying the evolution of wave-breaking events in the subtropics. Numerous studies have established the utility of CAS for studying mixing across the stratospheric polar vortex edge, and its ability to represent the fine scale, filamentary structures that are produced [e.g., *Norton*, 1994; *Waugh and Plumb*, 1994; *Waugh et al.*, 1994; *Mariotti et al.*, 1997]. Less attention, however, has been given to its potential for analyzing similar processes in the dynamically and radiatively more active region near the subtropical tropopause. Similarly, MesoNH has already been used in the study tropopause folds [e.g., *Donnadille et al.*, 2001], but its ability to represent the filamentary structures resulting from wave-breaking events has not yet been addressed.

The remainder of the paper is organized as follows. In section 2 we present observations and analyses that illustrate a particular case of stratospheric filamentation following a Rossby wave-breaking event at the subtropical tropopause. This case is investigated in more detail in sections 3 and 4 using the MesoNH and CAS models. Both the horizontal and the vertical structure of the filamentation are considered. In section 5 we discuss various implications of the modeling results, consider the extent to which the particular event examined is representative of other wave-breaking events, and present a brief climatology of such events based on all the MOZAIC flights over the tropical Atlantic. Conclusions are given in section 6.

2. Observed and Analyzed Data for November/December 1995

In this section, we present observations of anomalous ozone-rich air in the tropical upper troposphere by two MOZAIC flights and relate these, using global meteorological analyses, to the filamentation of stratospheric air following a wave-breaking event. The particular event presented here was selected over others because of the deep extension of the filament to equatorial latitudes, with MOZAIC measurements detecting high ozone anomalies at 3°S. See *Marenco et al.* [1998] and other papers in the special issue "First Results from the MOZAIC I Program" in *Journal of Geophysical Research, 103*, 25,631–25,737, 1998, for an overview of the MOZAIC program and for details of the instruments and measurement accuracies.

Anomalously high ozone values were measured by two MOZAIC flights over the tropical Atlantic on November 30, 1995, at 1800 UT and on December 1, 1995, at 0300 UT, the first flying from Frankfurt to Rio de Janeiro, the second returning from Rio de Janeiro to Frankfurt soon after. Several of the measured fields from each flight are shown in Figure 1, plotted as a function of latitude. The actual trajectories of the flights in the region of interest are indicated in Figure 2. As the first, southbound, flight passes south over the tropics, flying at an altitude of 10660 m (239 hPa), observed values of ozone mixing ratio rise steadily from around 35 ppbv at 12°N to around to 65 ppbv at 3°S. From here the observed ozone values rise more sharply to above 70 ppbv, reaching peaks of 90 ppbv near 4°S and 85 ppbv near 5°S, and then drop sharply again near 6°S. These peaks have ozone mixing ratio values significantly higher than the ambient tropospheric values. The horizontal scale of the anomaly defined, say, by ozone mixing ratio above 70 ppbv, between 3.4°S and 5.7°S, is about 300 km. Following this double peak, there is a gap of lower (below 60 ppbv) mixing ratio before values rise once more above 70 ppbv in a smaller scale, single peak, with a length scale of about 100 km at 8°S.

Consideration of the other fields shown in Figure 1 suggests that the anomalies are consistent with a positive local PV anomaly and hence with a locally lower equatorial tropopause [cf. *Hoskins et al.*, 1985, Figure 15a]. In particular, Figure 1b shows a sharp cyclonic change in the wind shear

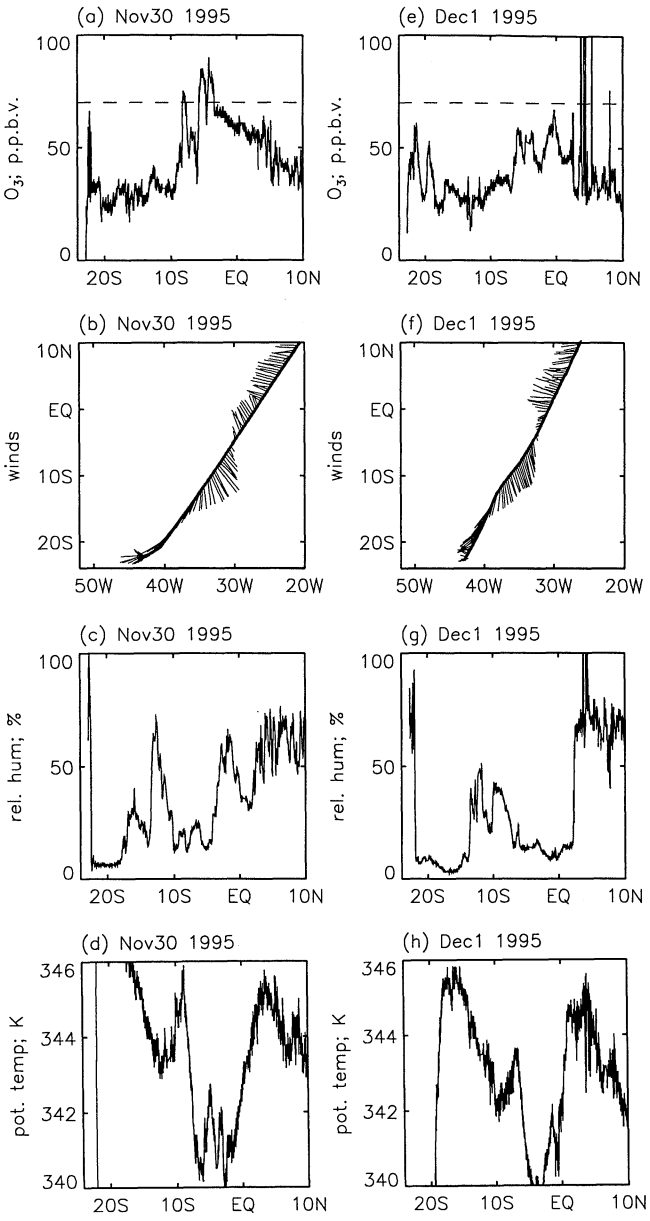

Figure 1. Flight data from MOZAIC flights on (a-d) November 30 (southbound flight) and (e-f) December 1, 1995 (northbound flight), plotted as a function of latitude: ozone (Figures 1a and 1e), wind speed and direction plotted along the flight trajectory (Figures 1b and 1f), relative humidity (Figures 1c and 1g), and potential temperature (Figures 1d and 1h).

with a near-zero minimum of wind speed centered on the strongest ozone peak, and Figure 1d shows a broad potential temperature minimum over the whole region with a local maximum also centered on the strongest ozone peak. Note also minima in relative humidity shown in Figure 1c coinciding with both the strong, double peaks and the weaker, single peak in the ozone. This small-scale structure will be considered in detail in sections 3–5 below.

The return, northbound, flight shows similar structure and anomalously high mixing ratios (Figures 1e–h), though these are lower than those measured by the southbound flight. Since the return trajectory is also a few degrees further west (see Figure 2), the lower mixing ratios suggest that the feature measured by the southbound flight is a local one. (The high ozone anomalies north of the equator in Figure 1e, and situated in a region of strong convective activity, were discussed in detail by *Suhre et al.* [1997]; they are not the focus of the present work.)

In support of the claim that the ozone anomalies are of stratospheric origin, Figure 2 shows potential vorticity (PV) from ECMWF analyses, with a spectral horizontal resolution of T213 (approximately 0.65° grid point resolution in the tropics), interpolated from pressure levels onto the 344 K insentrope. Also shown superposed is the water vapor channel image of Meteosat, near the time of the high-ozone measurements. The locations of the high-ozone measurements are indicated on each of the flight trajectories by the white diamonds. The 344 K isentrope corresponds approximately to the level of the flight before it enters the region of high ozone. From Figure 2 it is seen that the region of high ozone mixing ratios measured by the southbound flight corresponds to a filament of high PV (hereafter referred to as a PV filament) stretching equatorward from around 20°S. Similarly, the lower mixing ratios measured by the northbound flight can be understood as the result of the flight trajectory traversing the filament toward its northernmost extremity, where the signature of stratospheric air is weak. The Meteosat image, which indicates water vapor in a vertical region around 400 mbar, shows dry air over a much broader region, with a strong constrast a few degrees north of the equator giving an indication of the location of the intertropical convergence zone. Although the PV filament crosses north of the equator, it does not cross the convergence zone.

In Figure 3, snapshots of the ECMWF PV field on the 344 K isentrope at several times up to the time the southbound flight crosses the PV filament illustrate the development of the filament from a wave-breaking event at subtropical latitudes a few days earlier. On November 27 at 0000 UT the crest of a Rossby wave (i.e., the trough in the geopotential height) is located at 30°W. East of this, filamentary PV remnants from a previous wave-breaking event lie on the western edge of a stationary blocking anticyclone centered near 0°W. The combined influence of the wind field associated with these features contributes to the steepening of the PV contours defining the wave and its eventual breaking, with a filament of high PV air being drawn off the crest. Over the next 2 days, Figures 3b–3d, the filament drifts equatorward and is distended further by the strong deformation field induced by the blocking anticyclone. It remains longitudinally stationary while the crest of the parent wave moves off east. By the time of the flight crossing at 1800 UT on November 30, the filament extends from 25°S all the way to the equator and has become separated from the crest of the parent wave, which is now situated at 5°W.

3. Simulation with a Mesoscale Nonhydrostatic Model

We use a nonhydrostatic limited area general circulation model, MesoNH, based on the anelastic equations, with full physics to analyze the evolution of the PV filament described

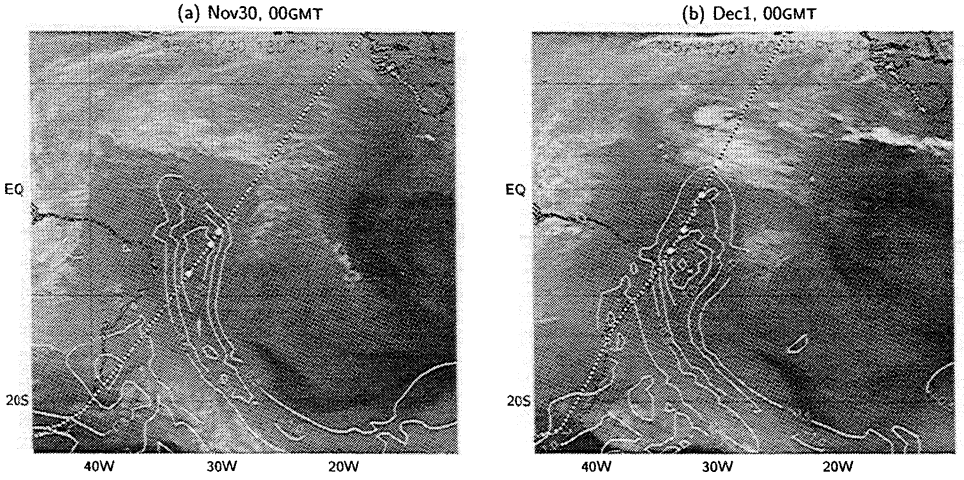

Figure 2. ECMWF PV on 344 K isentrope superimposed on Meteosat water vapor image, at the times of the (a) southbound and (b) northbound MOZAIC flights. The contour interval for the PV is -0.5 pvu where 1 pvu = 10^{-6} m^2 s^{-1} K kg^{-1}. The flight trajectories are shown dotted, and the maxima in the ozone measurements are indicated with white diamonds.

above. The model was jointly developed by Météo-France and the Centre National de Recherches Scientifiques and is described by *Lafore et al.* [1998] and *Mallet et al.* [1999]. The model uses T213 resolution ECMWF analyzed fields for initial and boundary conditions. The domain is the region 56°W–16°W, 53°S–20°N, ground–20 km, with a horizontal resolution of 40 km, and with 52 vertical levels, giving a resolution of approximtely 600 m in the free troposphere

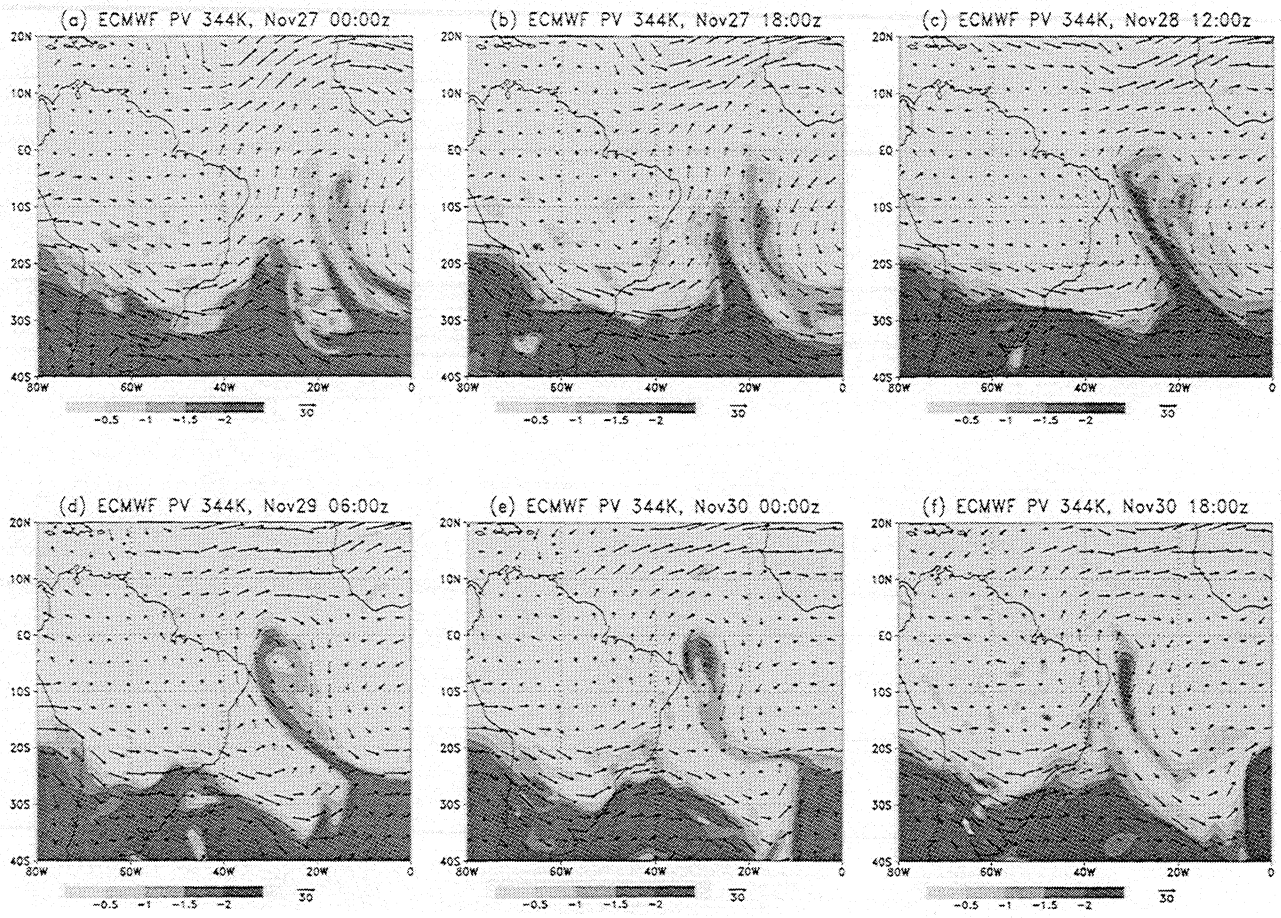

Figure 3. PV and wind fields on the 344 K isentrope from ECMWF analyses over the period November 27–30, 1995: (a) November 27 at 0000 UT, (b) November 27 at 1800 UT, (c) November 28 at 1200 UT, (d) November 29 at 0600 UT, (e) November 30 at 0000 UT, (f) November 30 at 1800 UT. Colorbar units are potential vorticity units.

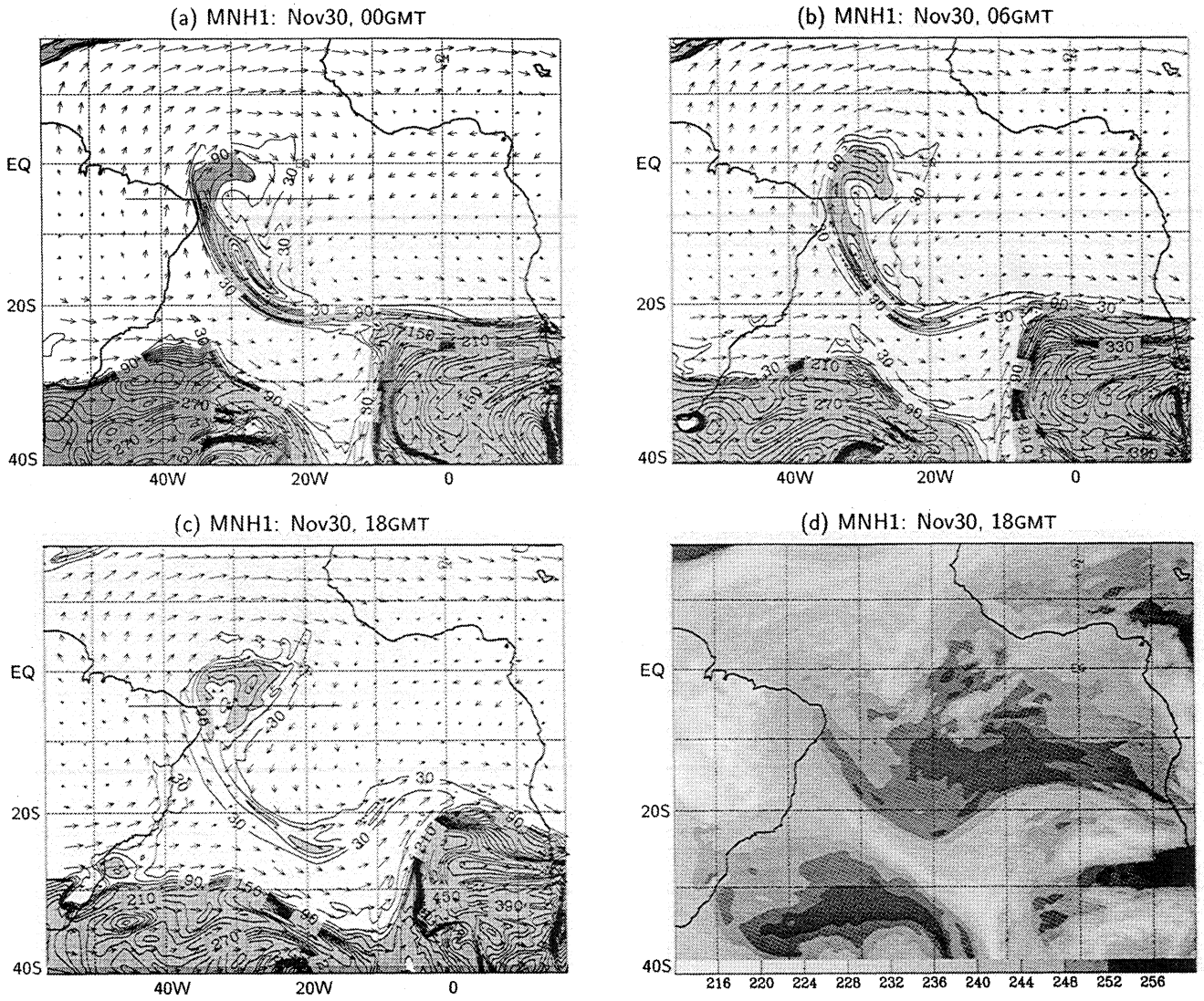

Figure 4. (a-c) Stratospheric passive tracer on the 344 K isentrope and (d) synthetic Meteosat brightness temperature (d) from the MesoNH simulation MNH1 initialized on November 29 at 0600 UT: (a) tracer field on November 30 at 0000 UT, (b) tracer field on November 30 at 0600 UT, (c) tracer field on November 30 at 1800 UT, and (d) brightness temperature on November 30 at 1800 UT.

and above and increasing resolution toward the ground. The physical parameterizations used include stratiform cloud and precipitation, convection, a planetary boundary layer, surface exchanges, radiation, and horizontal diffusion. In addition, a passive stratospheric tracer is included in the model, initialized with a mixing ratio α given in ppbv by $\alpha = 100q$ for $|q| \geq 0.75$, $\alpha = 20$ for $|q| < 0.75$, where q is the PV distribution in potential vorticity units (pvu) [*Ebel et al.*, 1991], with 1 pvu = 10^{-6} m^2 s^{-1} K kg^{-1}.

One objective of using this model is to obtain a dynamically consistent picture of the evolution and to improve on the horizontal and vertical resolution of the ECMWF analyses. Another objective is to use the passive statospheric tracer, a basic representation of ozone in the model, in conjunction with the PV as an indicator of air of stratospheric origin. A final objective is to assess the ability of the model to accurately represent the evolution of filamentary structures such as the one studied here. Since these structures are essentially advected upper level PV anomalies, they are associated with changes in the static stability of the troposphere below [*Hoskins et al.*, 1985]. It is anticipated therefore that future studies will use this model to investigate the relation between upper level filamentation and the triggering of deep convection in the troposphere.

We present the results of one simulation, MNH1, initialized on November 29 at 0600 and later remark on the sensitivity of the evolution to different initial times. At the initial time of the simulation the filament is already well formed, with some weak internal structure toward the filament tip (compare Figure 3d). The evolution of the filament can be seen in Figure 4a–c, which shows the stratospheric passive tracer on the 344 K isentrope for November 30 at 0000, 0600, and 1800 UT. It shows a roll up of the filament tip, similar to that hinted at in the ECMWF analyses (compare

Figure 3e) but beginning slightly later on the November 30 at 0600. By the time of the southbound flight the return branch of the filament roll up dominates the original filament (Figure 4c). The roll up also suggests the origin of the smaller scale (around 100 km width) peaks in the MOZAIC ozone data shown in Figure 1a. This will discussed more fully in section 5.1 below.

Validation of the larger scales of the simulation was provided by the geopotential height and wind fields on 250 hPa (not shown), which revealed broad agreement with both the ECMWF analyses and the MOZAIC wind data, with only a slight distortion of the overall geometery. Further, comparison of the synthetic water vapor brightness field calculated from the model by the method used by *Chaboureau et al.* [2000] with the Meteosat water vapor channel indicates broad agreement of the location of the Intertropical Convergence Zone and the dry air in the region of the filament (Figure 4d).

The vertical structure is illustrated in Figures 5a–d. This is a vertical cross section between 45°W and 15°W at latitude 5°S. The depth of the original filament branch is clearly visible in Figure 5a, spanning the whole region between the 340 K isentrope, just below the level of the flight, and the tropical tropopause above 370 K. The evolution of the roll up of the filament is also visible in Figures 5b–d. This exhibits a stronger vertical dependence, with the roll up beginning at lower altitudes on November 30 at 0600 UT and not developing high up until 1800 UT. Also evident at lower altitudes is the intensification of the return branch of the roll up and the weakening of the original branch, as seen in the

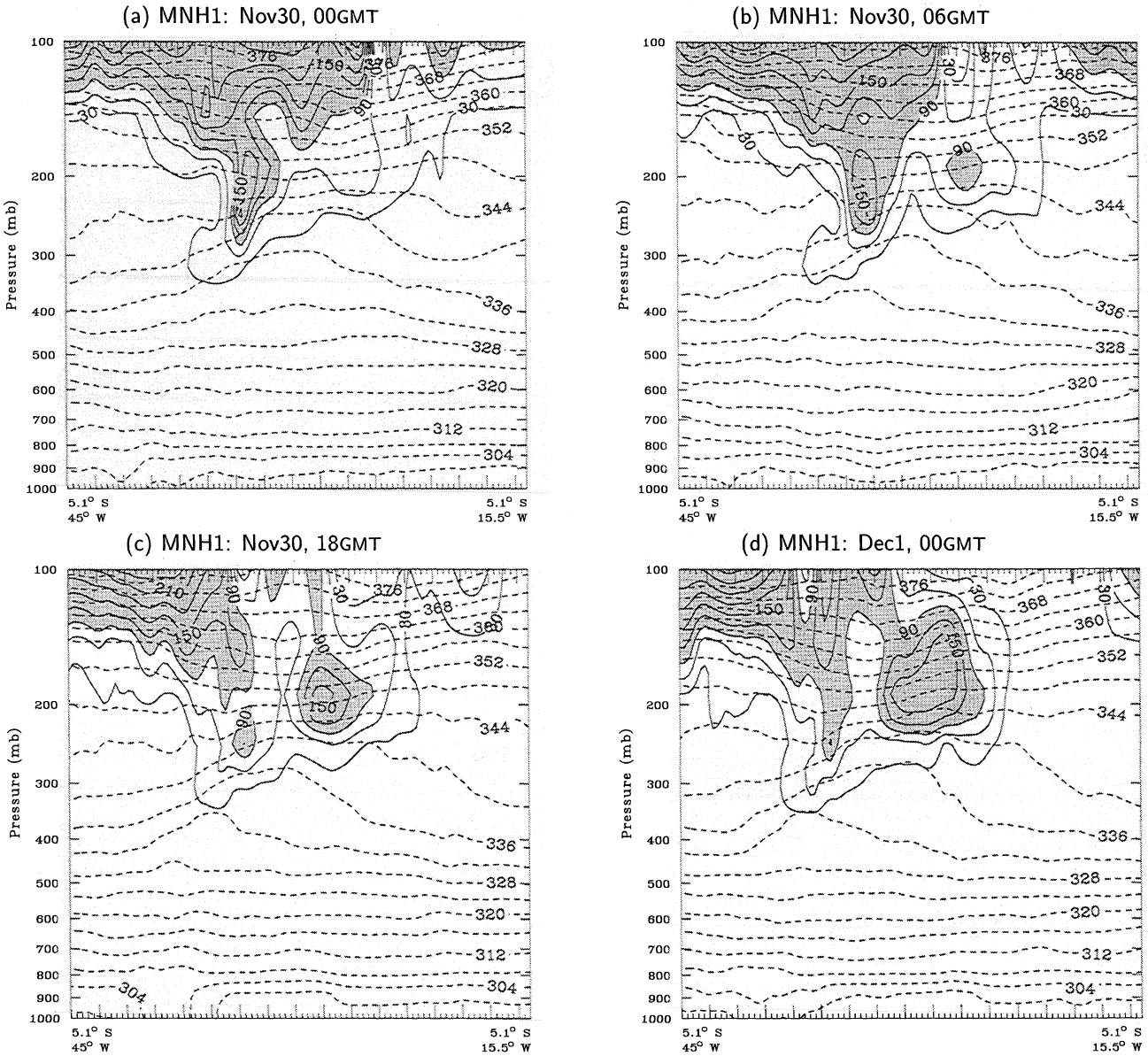

Figure 5. Stratospheric passive tracer on a vertical cross section at 5°S between 45°W and 15°W (as depicted by the line in Figure 4) from the MesoNH simulation MNH1 initialized on November 29 at 0600 UT: (a) on November 30 at 0000 UT, (b) on November 30 at 0600 UT, (c) on November 30 at 1800 UT, and (d) on December 1 at 0000 UT.

isentropic fields shown in Figure 4. The roll up thus has an approximate spiral or corkscrew form and is similar in character to the vertical structures found in idealized models of three-dimensional vortex dynamics [e.g., *Dritschel and Saravanan*, 1994]. We note that such an evolution is consistent with the wind field near the filament tip, which is induced primarily by the filament PV itself rather than the more distant large-scale PV field associated with the stratosphere.

Two other simulations were initialized on November 28 at 1200 UT (MNH2) and November 30 at 0000 UT (MNH3) 18 hours earlier and later than MNH1 to test the sensitivity to the initialization time. Similar behavior is observed but with some changes in the timing of events and in the vertical structure. For example, MNH2, which was initialized in the early stages of the filament evolution (Figure 3c), reproduced the subsequent filament evolution and roll up. The roll up, however, occurred slightly earlier than in MNH1, so that by the time of the southbound MOZAIC flight the resulting double structure was no longer present. On the other hand, MNH3, which was initialized in the late stages of the filament evolution (Figure 3e), followed the ECMWF analyses more closely through the later stages of the filament developement, around the time of the MOZAIC flights. We conclude that the MesoNH model is able to reproduce consistently the internal dynamics of the filament evolution, both in the early, roll up stage and in the later, decaying stage.

4. Simulation with a Contour Advection Model

In this section we use an isentropic Lagrangain advection technique, contour advection with surgery (CAS), developed by *Dritschel* [1989], to analyze the small-scale development of the filament. In the configuration used here, CAS uses externally imposed winds on an isentropic surface to materially advect an initial distribution of PV on that isentropic surface. Both the externally imposed advecting wind field and the PV are taken from T213 ECMWF 6-hourly analyses [e.g., *Mariotti et al.*, 1997]. The initial PV distribution is chosen on a particular day sometime before the wave-breaking event, and the advecting wind field is determined on that isentrope at each model time step by interpolating in time and space the ECMWF wind fields over a time interval from the initial time to some time after the end of the simulation. When scales become so small that the distance between contours is less than a threshold distance (here 20 km), surgery is applied to cut or join contours as appropriate. This configuration is similar to that used by *Dethof et al.* [1999] to investigate water vapor transport from the tropical troposphere to the lower stratosphere.

4.1. Representation of the Horizontal Evolution

Figure 6 shows results of a CAS simulation on the 344 K isentrope initialized on November 28 at 1200 UT at selected times (every 18 hours) from shortly after the initial time (Figure 6a) to the time of the southbound MOZAIC flight (Figure 6d). Dark shading represents stratospheric air with absolute PV values greater than 2 pvu. In Figure 6a the remains of the old filament resulting from the earlier wave-breaking event can be seen pressed against the right-hand side of the new developing filament. The stationary blocking anticyclone lies to the east of the filament and contributes to the wind field causing the extrusion of the new filament, as described in section 2 above. The event resembles a weakly supercritical wave-breaking event [see *Polvani and Plumb*, 1992], where the stagnation point in the wind field lies inside but close to the defining contours of the high PV region and a relatively small amount of high PV air is stripped away. By November 29 at 0600 UT the filament is well developed and the roll up of the filament end, similar to that described in sections 2 and 3, has started. By November 30 at 0000 UT, Figure 6c, the roll up of the filament end is well developed and the return branch has been stretched back down much of the length of the filament. Soon after, the -1.0 pvu contour separates from the main stratospheric reservoir. At this point the original connecting part of the filament has become so stretched out that all the higher PV air (absolute values above 1.5 pvu) has been advected around the northern tip of the filament and is being stretched out southward along its eastern edge. Note that the deformation field at the northern tip of the filament is weaker than that in the main part of the filament so that the high PV air there is less stretched out than that farther south. By the time of the MOZAIC flight on November 30 at 1800 UT, Figure 6c, there is a broad region of high PV air around 30°W, 3°S and a finer filament of high PV air that has been stretched farther southward following the roll up of the filament tip.

The general form of the filament produced by CAS is very similar to that shown in the ECMWF analyses (Figures 3c–3f) as is the timing of the roll up of the filament tip. In addition, the smaller scales of the return "subfilament" following the roll up show qualitative agreement with the smaller scale (100 km) ozone peaks seen in the MOZAIC data. This will be considered in more detail in section 5.1 below. Here we note the correspondence between the thin subfilament and the small second ozone peak, and between the broader region of high PV air around 30°W, 3°S and the stronger, double ozone peak.

4.2. Sensitivity to Initial Conditions

We consider the sensitivity of both the large and the small-scale evolution of the filament described above to changes in the initial time of the CAS simulations. Figures 7a–7c show the final fields, at the time of the southbound bound MOZAIC flight, of 3 CAS simulations initialized on November 29, 27 and 26 at 0000 UT. The corresponding field of the simulation initialized on November 28 at 1200 UT is in Figure 6d, while Figure 7d will be discussed below. In the following discussion we refer to these simulations as C28′ (Figure 6d) and C29, C27, C26 (Figures 7a–7c).

First consider the large-scale structure. The final position and general shape of the filament is similar between each of the four simulations, implying that these are determined by the externally imposed wind field (which is the same in each

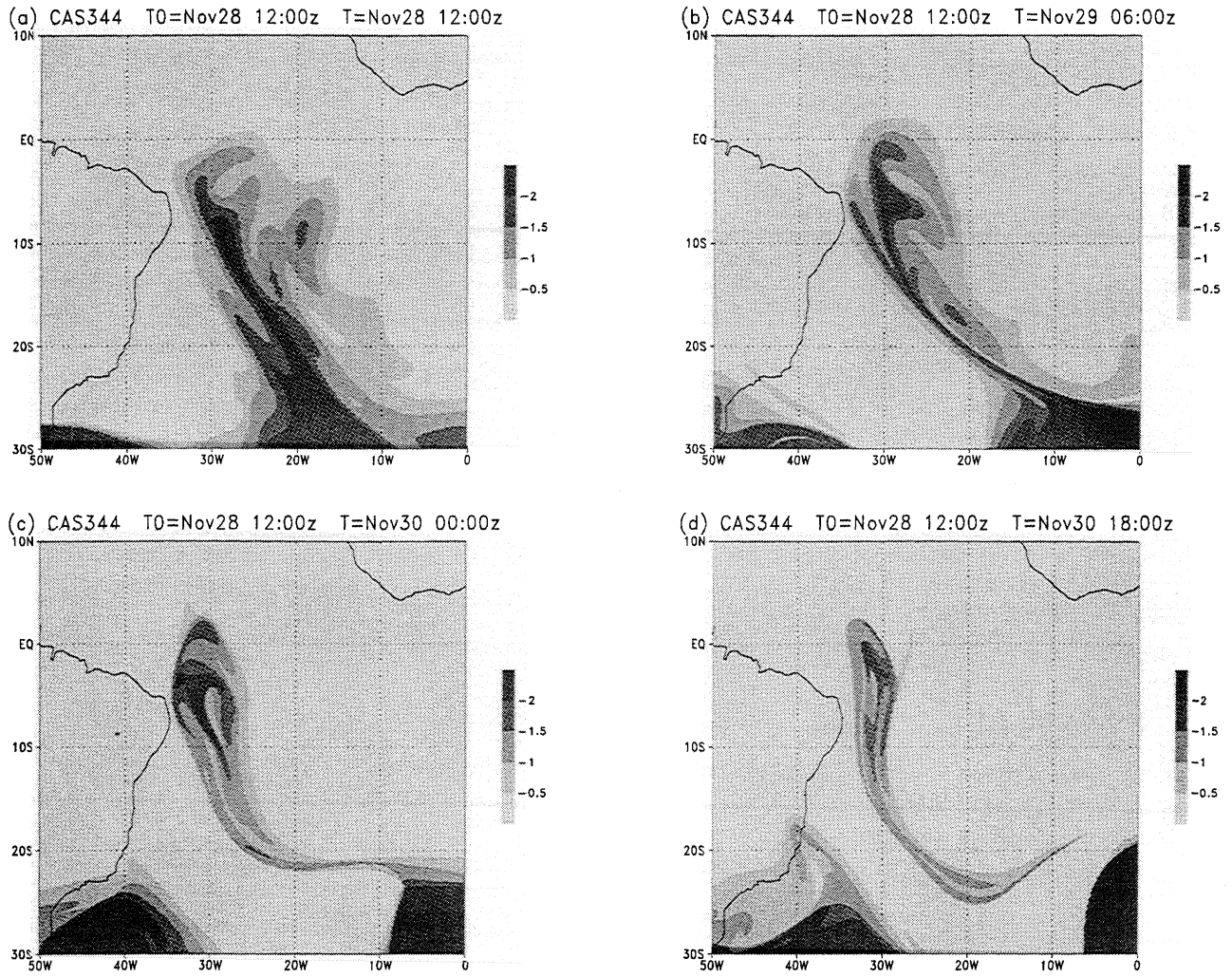

Figure 6. The CAS simulation C28′ initialized on November 28 at 1200 UT, PV field on 344 K: (a) on November 28 at 1200 UT (the initial time), (b) on November 29 at 0600 UT, (c) on November 30 at 0000 UT, and (d) on November 30 at 1800 UT (the time of southbound flight).

simulation) rather than by the particular distribution of the initial PV field (which varies). On the other hand, defining the strength of the filament as, say, the area integral of the PV over the filament, we see that the strength of the filament is weaker, the earlier the initial time. This could either be a result of the divergent component of the advecting winds, or else details of the PV fields at the initial times of the simulations. (It was verified that the surgery algorithm in the CAS model was not responsible.)

Next consider the creation of small scales, or "subfilaments", within the filament, important for determining the mixing rate of stratospheric air into the troposphere. Again considering Figure 6d and Figures 7a–7c, we see there is a distinct change in the character of the filament between the simulation initialized on November 29, C29 in Figure 7a, and those initialized earlier. As a crude indicator of the small-scale structure, one may count the number of extrema in the PV field along a line of latitude cutting through the main part of the filament, for example, a line at 5°S: there is a jump from three extrema for C29 to seven extrema for C28′. Simulations initialized earlier, C27 and C26, contain similar small-scale structure except that the combination of the weaker filament strength and the surgery algorithm of the model eliminates some of the finer details. A similar picture is seen by considering the PV field along the southbound MOZAIC flight trajectory (see Figure 9c). The wind field during the filament development gives a turn around time of the filament of about 2 days (e.g., Figure 6b–d), which is also the length of time it takes the filament to develop from its formation from a wave-breaking event. Thus the lack of fine scales in C29 should not be too surprising. Alternatively, one could argue that the sharp difference between C29 and C28′ suggests a minimum timescale for the development of small scales within a filament evolution, this being of the order of the filament turn around time.

Finally, we mention a recent development of the CAS model to include a basic representation of diabatic processes [*Mariotti*, 1997]. Every 6 hours the CAS PV field is com-

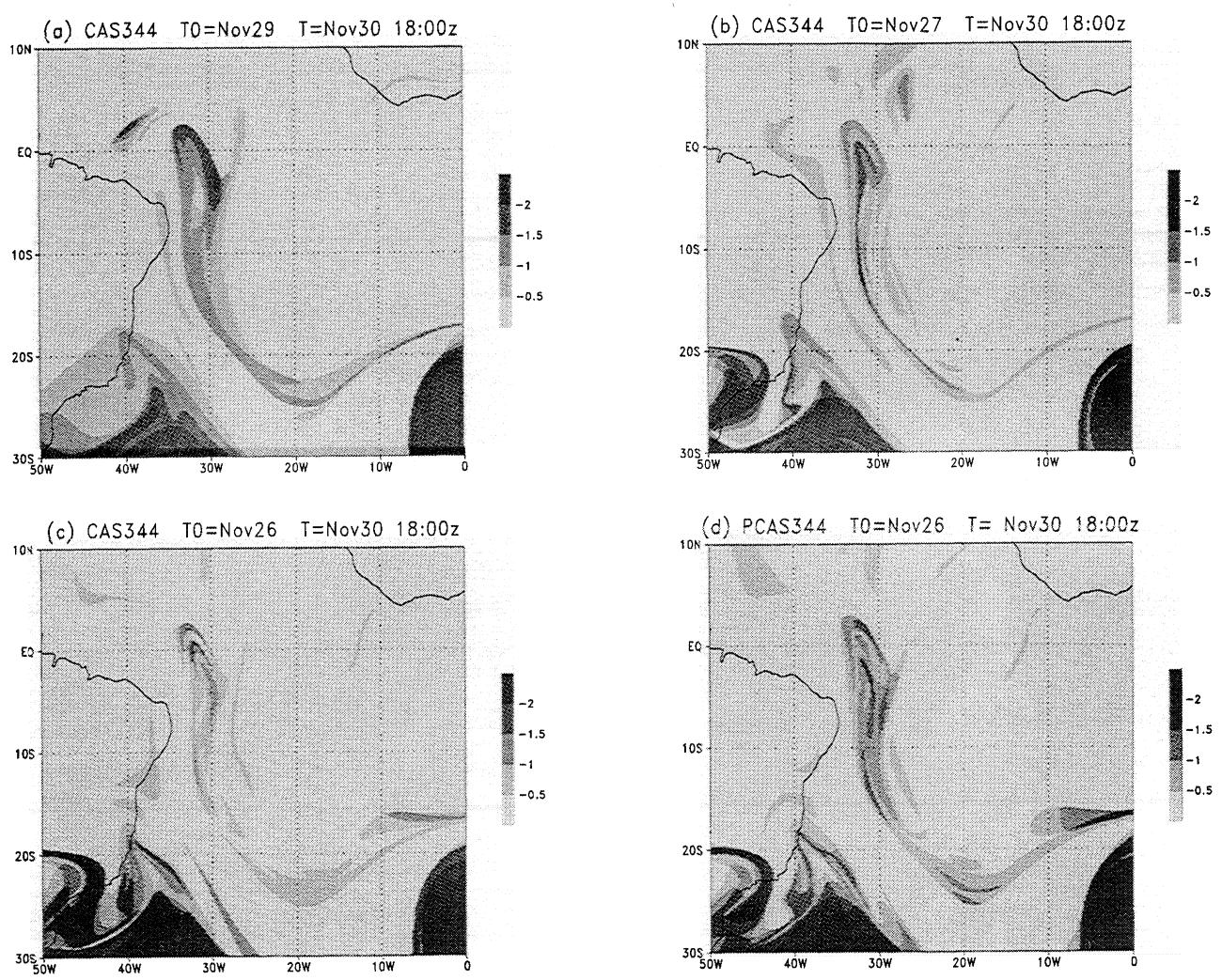

Figure 7. (a-c) The CAS simulations C29, C27, C26 initialized on November 29, 27, 26 and (d) the pseudo diabatic CAS simulation C26D initialized on November 26; PV field on 344 K on November 30 at 1800 UT (the time of southbound flight).

pared with the PV field from the ECMWF analyses. The large-scale difference is calculated from the lowest spectral modes and is used to calculate a "pseudo wind field" that advects the PV isocontours in a second advection stage. The pseudo wind field is calculated such that the second advection stage gives a large-scale CAS PV field that is in better agreement with the large-scale PV field from the analyses; thus it contains a representation of the diabatic evolution of the PV. Calculating the pseudo wind field using only the large-scale components of the PV fields ensures that the small scales generated by the CAS model are unaffected by the second advection stage. Figure 7d shows an example of the effect of including such a diabatic representation for a simulation initialized on November 26, which we refer to as C26D. In this simulation, the pseudo wind was calculated using the T41 component of the CAS/observed PV field difference. Comparing it to C26 in Figure 7c, it is clear that a much stronger filament is produced, in better agreement with the large-scale ECMWF analyses, and of similar strength to the simulation C29 initialized much later. On the other hand, C26D contains more small-scale structure than C29, and qualitatively at least, suggests a better agreement with the small scales seen in the MOZAIC ozone data. Though we do not pursue this further here, we note that the technique has potential applications for allowing an earlier initialization of the CAS simulation and hence more time for small-scale development, while maintaining accuracy at large scales.

4.3. Vertical Dependence

It can be seen from Figure 5 that the wave-breaking event and resulting filament extends in the vertical downward to about the 340 K isentropic surface. This is consistent with CAS simulations on that level (Figure 8a), which showed a significantly weaker filament evolution than that at 344 K. Despite the weaker filament, however, the same roll up of the filament tip on November 29 was found, and until November 30 the evolution closely follows that of C28′ on the 344 K

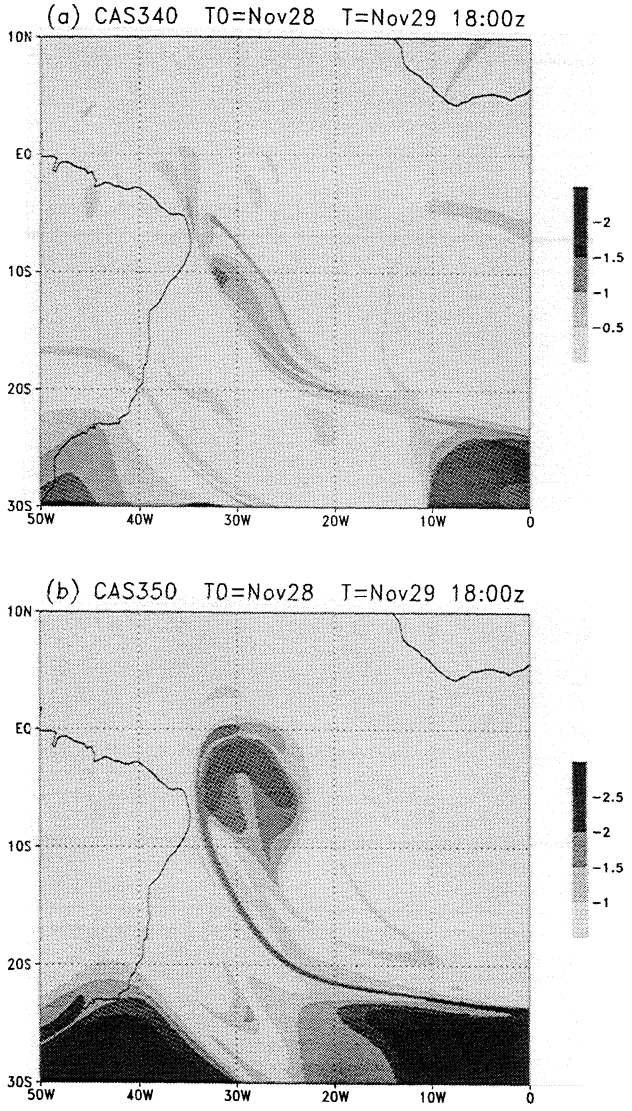

Figure 8. CAS simulations initialized on November 28th at 0000 UT PV field on (a) 340 K and (b) 350 K, on November 29 at 1800 UT.

isentropic surface described in section 4.2 above. On the 350 K isentropic surface the evolution is again similar to that on 344 K, Figure 8b, with a somewhat stronger roll up of the filament tip.

At higher levels, 360 K and 370 K (not shown), although the filament is still present, other strong PV anomalies begin to dominate the picture. These can be traced back through the CAS evolution and the ECMWF analyses and can be seen to originate from isolated regions of anomalously strong PV at earlier times in the analyses. These are retained in the CAS simulations but generally dissipate in the analyses within a day or two. Although it is possible that the anomalies are real and are subject to strong diabatic processes in their subsequent evolution, it seems more likely that they are simply artifacts of the analyses or of the vertical interpolation. Caution is therefore necessary when interpreting the CAS results at these higher levels.

5. Discussion

5.1. Comparisons of the Models and Data

The roll up of the filament tip was seen as a robust feature in both the MesoNH and the CAS simulations. We note that the roll up in MNH1 is strongest on the 344 K to 360 K isentropes (Figure 5c), which is in agreement with the CAS simulations on the 340 K, 344 K, and 350 K surfaces (Figure 6d and Figures 8a and 8b). Although the lower (T213) resolution analyses represent the filament on the 30th at 1800 UT by a single, stretched out maximum of PV (Figure 3f), consideration of Figure 3e and the PV fields at the intermediate times (0600 UT and 1200 UT, not shown) do suggest a similar roll up event. In particular, the rightmost maximum in Figure 3e corresponds to the return branch, and this then moves south to become the single maximum in Figure 3f.

The limiting factor in both the analyses and the MesoNH model is the inclusion of horizontal diffusion, necessary to retain model stability. In MesoNH this takes the form

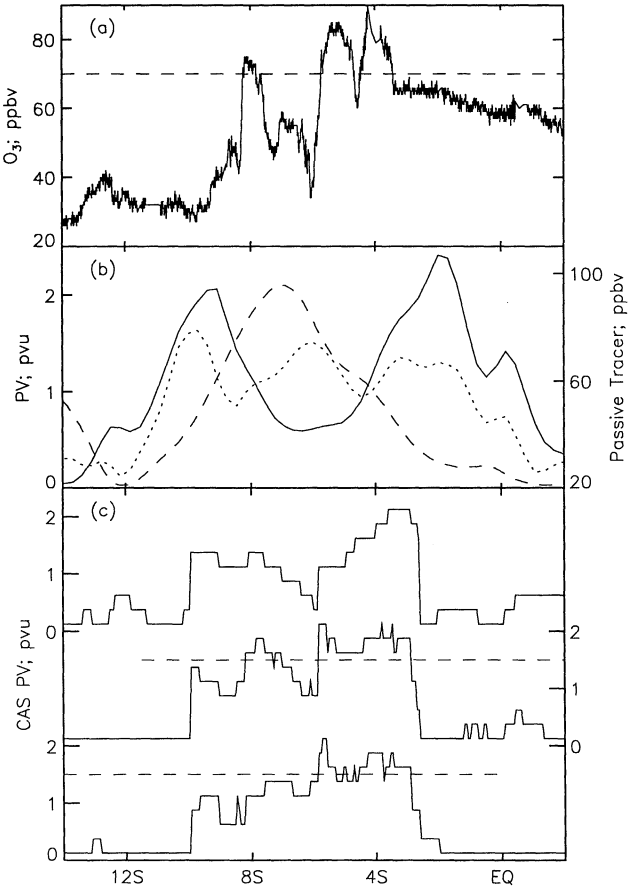

Figure 9. Comparison of (a) MOZAIC ozone data from the flight on November 30 with PV/ozone from ECMWF, MesoNH, and CAS interpolated onto the flight trajectory: (b) MNH1 MesoNH simulation PV (solid) and stratospheric passive tracer (dotted), and ECMWF PV (dashed), interopolated in space onto the flight trajectory from the November 30 1800 UT fields; (c) PV from the C29, C28′, C28 CAS simulations (from top to bottom) interopolated in space onto the flight trajectory from the November 30 1800 UT fields.

of a scale-selective, ∇^4 hyperdiffusion acting on the prognotic variables. This diffusion is such that length scales shorter than $L(T_{\text{def}})$, where T_{def} is a characteristic deformation timescale, will not persist in the simulation. Considering the velocity field across the filament, for example, near 30°W, 15°S, we can estimate a deformation timescale of approximately 5×10^4 s, giving $L \sim 240$ km. Thus we would expect the fine scales generated along the filament length in Figures 4a and 4b to be removed by the model diffusion during the course of the simulation. This explains the weaker filament shown in Figure 4c. On the other hand, the deformation field at the filament tip is somewhat weaker (compare section 4.1 above), with the result that the double structure that develops from the roll up persists for longer, until December 1 (Figure 5).

To compare the small-scale structure in the MOZAIC data, that is, the ozone peaks with length scale $\sim$ 100 km, with the MesoNH and CAS simulations, we plot the model output along the flight trajectory in Figure 9. Comparing Figure 9a with Figure 9b (solid and dotted lines), we see there is some correspondence between the PV and passive tracer from the MNH1 simulation and the MOZAIC ozone. Although the structure is more stretched out in MNH1, there is still evidence that the small-scale structure in the MOZAIC data is related to the roll up of the filament tip described above. On the other hand, the PV from the analyses (dashed line in Figure 9b) shows no internal structure, with a single PV maximum located near the ozone anomalies.

Figure 9c shows the PV along the trajectory for the CAS simulations C29, C28′, and C28 (descending). Although these fields are taken from the 344 K isentropic surface and so not exactly along the flight trajectory, there is nevertheless good qualitative agreement with the MOZAIC ozone. Note, however, that the double peak structure in C29 is fundamentally different from the structures in the simulations C28′ and C28 initialized earlier. In C29 the peak at 9°–10°S is associated with the original filament, whereas for the earlier simulations most of the structure is associated with the differential stretching of the subfilament created after the roll up event. Since the filament is already several days old by the time of the MOZAIC flight, we believe the earlier CAS simulations give a better representation of the origin of the ozone anomalies.

5.2. Other Filamentation Events

Numerous example of filament formation following wave-breaking events have been found using the MOZAIC data (see section 5.3 below) and the ECMWF analyses. The above event was selected for analysis because of the deep equatorward intrusion, but it is important to assess to what extent it is representative of others. We do not present an exhaustive analysis here but instead describe briefly two other events that illustrate interesting possible differences in filament evolution.

The first of these is closer to the strongly supercritical case of *Polvani and Plumb* [1992], with a stagnation point deeper inside stratospheric reservoir and stronger wave breaking.

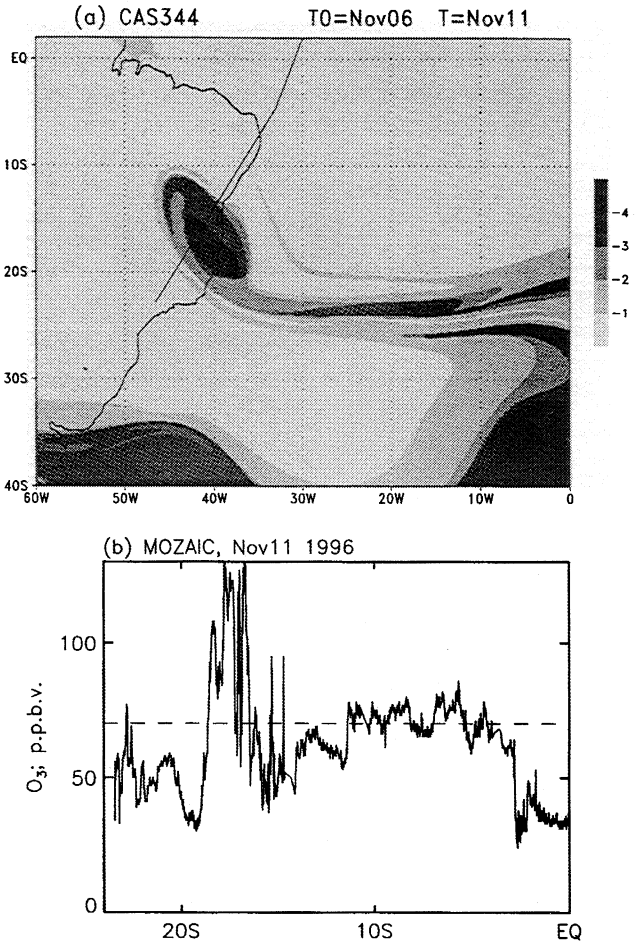

Figure 10. (a) PV on November 11, 1996, at 0000 UT from a CAS simulation initialized on November 6, 1996 at 0000 UT and (b) ozone from the MOZAIC flight on November 11, 1996. The line in Figure 10a shows the approximate flight trajectory.

More high PV air is drawn off the stratospheric reservoir, resulting in a larger filament. The subsequent evolution of this filament shows a similar roll up of the filament tip as before but is much more pronounced. After the initial development the roll up forms a strong, coherent vortex patch, or cutoff low (COL), as shown in Figure 10a, that persists for several days (note the different scale in the shading). The COL has little internal structure, the smaller scale, subfilamentation being restricted to the edge of the COL and to the orginal filament stretched between the COL and the stratosphere. The lack of internal structure is confirmed by the MOZAIC ozone measurements in Figure 10b, which shows a strong, single peak, with smaller scale structure on the flanks.

The second event is an example of weaker wave breaking. In this case, rather than forming a strong filament with internal dynamics, we see instead a gradual and persistent stripping, or erosion, of high PV air from the crest of the wave as it propagates east (Figure 11a). This erosion results in a broad, diffuse region of -0.5 and -1.0 pvu air situated between the tropopause and the equator and between 60°W and 0°W. The MOZAIC ozone data from a flight crossing this

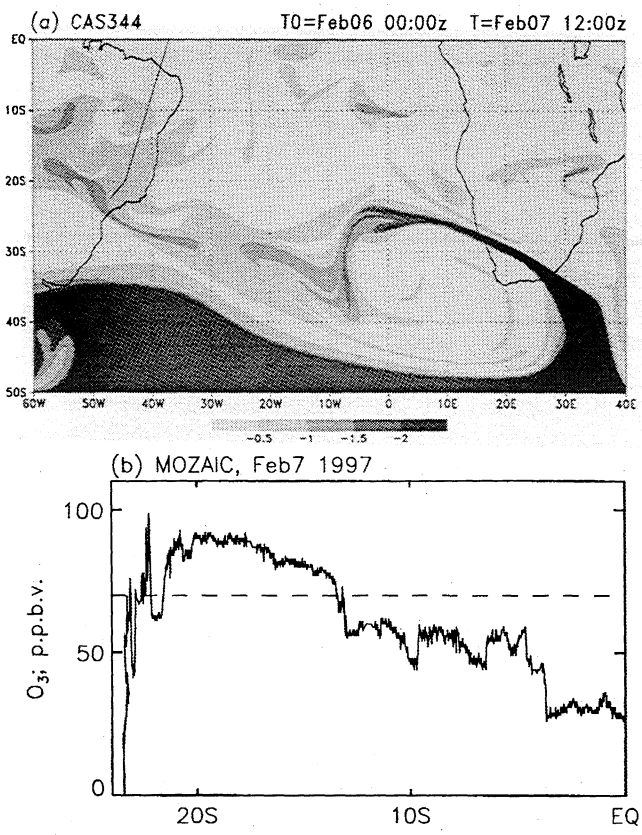

Figure 11. As Figure 10, but for February 7, 1997 at 1200 UT, with a CAS simulation initialized on February 6, 1997, at 0000 UT.

region on the same day (Figure 11b) are in good agreement, with high ozone values over a broad area and little smaller scale structure. Further, the MOZAIC wind data (not shown) are characterized by weak winds with very little shear, again indicating that the high ozone values are not associated with a strong, coherent PV anomaly.

5.3. Frequency of Wave-Breaking Events Derived from MOZAIC Data

The irregular distribution in space and time of the MOZAIC flights, governed by commercial strategies, makes an objective analyses of high-ozone anomalies difficult [*Cammas et al.*, 1998]. For example, a filament of high-ozone air resulting from a wave-breaking event may last several days, or there may be more than one flight traversing it. With this in mind, we searched the MOZAIC database of flights between Europe and South America for all ozone anomalies between 0°S and 22°S. A high-ozone event was defined to occur if measured ozone values remained above a given threshold value over a given threshold length of the flight trajectory. An additional criterion based on the observed wind direction along the trajectory was also used to refine the search, selecting only those high-ozone events associated with a wind signature typical of a filament of high PV air. Various threshold values and trajectory lengths were used to verify the robustness of the results. Attention was restricted to segments of the flight trajectory at altitudes higher than 10 km, to avoid high-ozone events associated with subtropical foldings sometimes observed in the ascents/descents at the South American end of the flights.

To reduce the effect of the irregular density of the MOZAIC flights, we sampled all flights between 1994 and 2000 and formed a composite year, arriving at a density of between 50 and 85 flights each composite month. All flights in a given month that contained an event satisfying the selection criteria were counted and divided by the total number of flights for that month. The ratio for each month is displayed in Figure 12, using an ozone threshold value of $O_3^T = \min(50, \langle O_3 \rangle + 20)$ over a threshold trajectory length of $L_{\text{ozo}}^T = 70$ km. It shows a minimum of high-ozone events in Southern Hemisphere (SH) autumn and winter and a maximum in SH spring and summer. Adding the additional selection criterion that the wind direction must change direction by at least $\phi^T = 90°$ within a trajectory length of $L_{\text{wind}}^T = 230$ km centered on the ozone maximum changes the structure slightly, shifting the October maximum to November and emphasizing the February maximum. The patterns were found to be robust to changes in the threshold values O_3^T, L_{ozo}^T, ϕ^T, L_{wind}^T, with overall amplitudes weakening for higher threshold values.

These results are in approximate agreement with the Southern Hemisphere results of the climatological studies of subtropical Rossby wave breaking by *Postel and Hitchman* [1999] and *Waugh and Polvani* [2000], though with some notable differences. In particular we find a local minimum in December/January that was not present in the other studies.

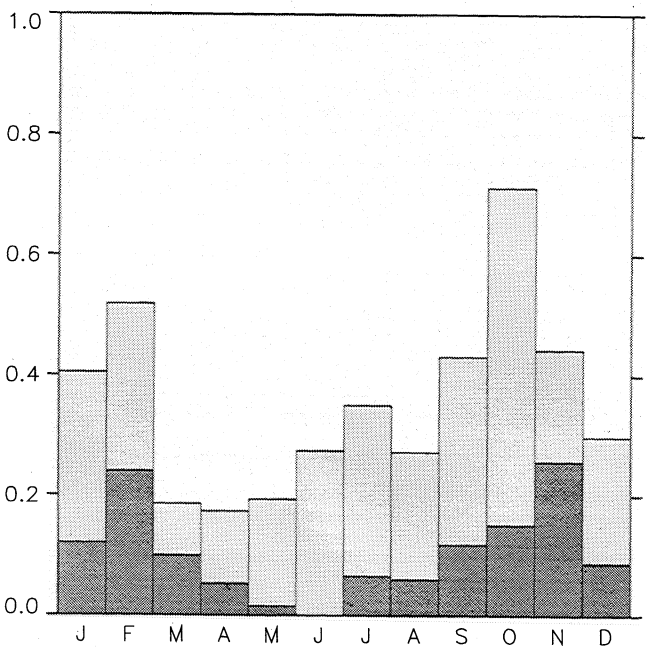

Figure 12. Occurrence of high-ozone events in all tropical Atlantic flights in the MOZAIC data set, for each month as a fraction of the total number of tropical Atlantic flights: high-ozone events defined by ozone values alone (light grey) and high-ozone events defined by ozone values and wind direction (dark grey). See text for details.

There are several possible explanations. For example, the latitude range from which we selected the high-ozone events was 0°S to 22°S, constrained by the southernmost latitude of the MOZAIC flight trajectories. The poleward displacement of the subtropical jet stream in the summer, and the corresponding poleward displacement of the high PV gradients defining the tropopause around the 340–350 K isentropic surfaces, could result in Rossby wave-breaking events occurring too far south in December/January to be present in our data. Another possibility is the longitudinal localization of the present study, for example, as compared with the zonal average taken by *Postel and Hitchman* [1999, Figure 3]. Finally, processes other than Rossby wave breaking, such as tropopause foldings and cutoff lows, could be responsible for the high frequency of high-ozone events detected in October/November in this study.

6. Conclusions

A search of all the MOZAIC flights crossing the tropical Atlantic has revealed signatures of wave breaking and filamentation of stratospheric air into the subtropical troposphere. These events are characterized by anomalously high tropospheric ozone values and low humidity, as well as wind and potential temperature fields consistent with stratospheric PV values. ECMWF analyses and two numerical models were used in this study to verify the stratospheric origin of the high-ozone air and to investigate the evolution of filaments of stratospheric air resulting from Rossby wave breaking near the tropopause (as opposed to the more widely investigated tropopause folding processes). The high-ozone events occurred in a significant fraction of the total number of MOZAIC flights over the southern tropical Atlantic region, with the largest number of events in spring and summer.

The model results from both MesoNH and CAS indicate that the small-scale structure in the MOZAIC ozone data results from the internal dynamics of a filamentary structure that is left behind after a Rossby wave-breaking event. Although diffusion prevented the MesoNH model from retaining the smallest scales produced, it was nonetheless able to represent qualitatively the roll up of the filament tip. The vertical structure obtained by MesoNH was suggestive of the vertical structure sometimes seen in idealized models of vortex evolution. The small scales produced by CAS were in good agreement with the MOZAIC ozone data, provided the initial time of the simulation was long enough before the flight for the small scales to develop. Finally, consideration of two other cases showed the dependence of the filament evolution on the strength of the wave-breaking event, with the formation of a strong, coherent vortex in the strong wave-breaking case, and the gradual erosion of high PV air in the weak wave-breaking case.

Crucial to quantifying the stratosphere-troposphere exchange associated with these features is an understanding of the small-scale generation and evolution within the larger scale filamentary structures, and the associated timescales for mixing into the troposphere. Our study has shown a large range of small-scale development depending on the strength of the wave-breaking event prior to the filamentation. The mixing timescales in these different cases will be correspondingly diverse. On the basis of the frequency of the wave-breaking events, and of the general small-scale development suggested by numerical modeling studies, we can infer a significant contribution by these processes to the global stratosphere-troposphere exchange. It is anticipated that future work providing quantitative estimates of mass transport arising from stratospheric intrusions of the type examined here will build on the above results.

Acknowledgments. The authors would like to thank Bernard Legras for providing the source code of the CAS model, the MOZAIC program for providing the flight measurements, ECMWF for providing the analyses and the Meteosat images, and Jean-Pierre Chaboureau for providing Figure 4d. Finally, we thank two anonymous reviewers for constructive comments that significantly improved the structure of the paper. Financial support was provided by the European Commission through the TRACAS project under contract ENV4-CT97-0546.

References

Appenzeller, C., and H. C. Davies, Structure of stratospheric intrusions into the troposphere, *Nature*, *358*, 570–572, 1992.

Appenzeller, C., H. C. Davies, and W. A. Norton, Fragmentation of stratospheric intrusions, *J. Geophys. Res.*, *101*, 1435–1456, 1996.

Baray, J.-L., V. Daniel, G. Ancellet, and B. Legras, Planetary-scale tropopause folds in the southern subtropics, *Geophys. Res. Lett.*, *27*, 353–356, 2000.

Bithell, M., L. J. Gray, and B. D. Cox, A three-dimensional view of the evolution of midlatitude stratospheric intrusions, *J. Atmos. Sci.*, *56*, 673–688, 1999.

Cammas, J.-P., S. Jacoby-Koaly, K. Suhre, R. Rosset, and A. Marenco, Atlantic subtropical potential vorticity barrier as seen by Measurements of Ozone by Airbus In-Service Aircraft (MOZAIC) flights, *J. Geophys. Res.*, *103*, 25681–25694, 1998.

Chaboureau, J.-P., J.-P. Cammas, P. Mascart, J.-P. Pinty, C. Claud, R. Roca, and J.-J. Morcrette, Evaluation of a cloud system life-cycle simulated by Meso-NH during FASTEX using METEOSAT radiances and TOVS-3I cloud retrievals, *Q. J. R. Meteorol. Soc.*, *126*, 1735–1750, 2000.

Chen, P., Isentropic cross-tropopause mass exchange in the extratropics, *J. Geophys. Res.*, *100*, 16,661–16,673, 1995.

Dethof, A., A. O'Neill, J. M. Slingo, and H. G. J. Smit, A mechanism for moistening the lower stratosphere involving the Asian summer monsoon, *Q. J. R. Meteorol. Soc.*, *125*, 1079–1106, 1999.

Diab, R. B., et al., Vertical ozone distribution over southern Africa and adjacent oceans during SAFARI-92, *J. Geophys. Res.*, *101*, 23,823–23,833, 1996.

Donnadille, J., J.-P. Cammas, P. Mascart, D. Lambert, and R. Gall, FASTEX IOP18: A very deep tropopause fold. Part I: Modelling with a passive stratospheric tracer, *Q. J. R. Meteorol. Soc.*, 2001, in press.

Dritschel, D. G., Contour dynamics and contour surgery: numerical algorithms for extended, high-resolution modelling of vortex dynamics in two-dimensional, inviscid, incompressible flows, *Comput. Phys. Rep.*, *10*, 78–146, 1989.

Dritschel, D. G., and R. Saravanan, Three-dimensional quasi-geostrophic contour dynamics, with an application to stratospheric vortex dynamics, *Q. J. R. Meteorol. Soc.*, *120*, 1267–1297, 1994.

Ebel, A., H. Hass, H. J. Jakobs, M. Laube, M. Memmesheimer, A. Oberreuter, H. Geiss, and Y.-H. Kuo, Simulation of ozone

intrusion caused by a tropopause fold and cut-off low, *Atmos. Environ.*, *25A*(10), 2131–2144, 1991.

Gouget, H., J.-P. Cammas, A. Marenco, R. Rosset, and I. Jonquiéres, Ozone peaks associated with a subtropical tropopause fold and with trade wind inversion: A case study from the airborne campaign TROPOZ II over the Caribbean in winter, *J. Geophys. Res.*, *101*, 25,979–25,993, 1996.

Haynes, P. H., and E. F. Shuckburgh, Effective diffusivity as a diagnostic of atmospheric transport, II, Troposphere and lower stratosphere, *J. Geophys. Res.*, *105*, 22,795–22,810, 2000.

Holton, J. R., P. H. Haynes, M. E. McIntyre, A. R. Douglass, R. B. Rood, and L. Pfister, Stratosphere–troposphere exchange, *Rev. Geophys.*, *33*, 403–439, 1995.

Hoskins, B. J., M. E. McIntyre, and A. W. Robertson, On the use and significance of isentropic potential-vorticity maps, *Q. J. R. Meteorol. Soc.*, *111*, 877–946, 1985.

Lafore, J.-P., et al., The Meso-NH atmospheric simulation system, I, Adiabatic formulation and control simulations: Scientific objectives and experimental design, *Ann. Geophys.*, *16*, 90–109, 1998.

Mallet, I., J.-P. Cammas, P. Mascart, and P. Bechtold, Effects of cloud diabatic heating on the early development of the FASTEX IOP17 cyclone, *Q. J. R. Meteorol. Soc.*, *125*, 3439–3467, 1999.

Marenco, A., et al., Measurements of ozone and water vapor by Airbus in-service aircraft: The MOZAIC airborne program, an overview, *J. Geophys. Res.*, *103*, 25,631–25,642, 1998.

Mariotti, A., Etude de la dynamique du vortex polaire stratospherique et des processus de transport, Ph.D. thesis, Lab. de Météorol. et Dyn., École Normal Supérior, Paris, 1997.

Mariotti, A., M. Moustaoui, B. Legras, and H. Teitelbaum, Comparison between vertical ozone soundings and reconstructed potential vorticity maps by contour advection with surgery, *J. Geophys. Res.*, *102*, 6131–6142, 1997.

McIntyre, M. E., The stratospheric polar vortex and sub-vortex: Fluid dynamics and midlatitude ozone loss, *Philos. Trans. R. Soc. London*, *352*, 227–240, 1995.

Norton, W. A., Breaking Rossby waves in a model stratosphere diagnosed by a vortex-following coordinate system and a technique for advecting material contours, *J. Atmos. Sci.*, *51*, 654–673, 1994.

Polvani, L. M., and R. A. Plumb, Rossby wave breaking, microbreaking, filamentation and secondary vortex formation: The dynamics of a perturbed vortex, *J. Atmos. Sci.*, *49*, 462–476, 1992.

Polvani, L. M., D. W. Waugh, and R. A. Plumb, On the subtropical edge of the stratospheric surf zone, *J. Atmos. Sci.*, *52*, 1288–1309, 1995.

Postel, G. A., and M. H. Hitchman, A climatology of Rossby waves breaking along the subtropical tropopause, *J. Atmos. Sci.*, *56*, 359–373, 1999.

Suhre, K., J.-P. Cammas, P. Nédelec, R. Rosset, A. Marenco, and H. G. J. Smit, Ozone-rich transients in the upper equatorial Atlantic troposphere, *Nature*, *388*, 661–663, 1997.

Waugh, D. W., and R. A. Plumb, Contour advection with surgery: A technique for investigating finescale structure in tracer transport, *J. Atmos. Sci.*, *51*, 530–540, 1994.

Waugh, D. W., and L. M. Polvani, Climatology of intrusions into the tropical upper troposphere, *Geophys. Res. Lett.*, *27*, 3857–3860, 2000.

Waugh, D. W., et al., Transport of material out of the stratospheric Arctic vortex by Rossby wave breaking, *J. Geophys. Res.*, *99*, 1071–1088, 1994.

J.-P. Cammas, P. Mascart, R. K. Scott, and C. Stolle Laboratoire d'Aérologie, UMR 5560, Observatoire Midi Pyrénées, 14 Av. E. Belin, 31400 Toulouse, France. (camjp@aero.obs-mip.fr; scor@aero.obs-mip.fr)

(Received July 26, 2000; revised December 19, 2000; accepted December 27, 2000.)